The Influence of Liquid Conductivity on Electrical Breakdown and Hydrogen Peroxide Production in a Nanosecond Pulsed Plasma Discharge Generated in a Water-film Plasma Reactor

Huihui Wang [1], Robert J. Wandell [1], Kosuke Tachibana [2], Jan Voráč [3] and Bruce R. Locke [1]

[1]Department of Chemical and Biomedical Engineering, FAMU-FSU College of Engineering, Florida State University, Tallahassee, FL 32310-6046, United States

[2] Department of Innovative Engineering, Faculty of Science and Technology, Oita University, 700 Dannoharu, Oita city, Oita 870-1192, Japan

[3]Department of Physical Electronics, Masaryk University, Kotlářská 2, 61137 Brno, Czechia

ABSTRACT

The influence of liquid conductivity on electrical breakdown and hydrogen peroxide (H_2O_2) production in a nanosecond pulsed filamentary discharge generated in a water film plasma reactor was investigated over the liquid conductivity range from 0.01 mS/cm to 36 mS/cm by adding KCl to deionized (DI) water and using helium and argon as carrier gases. The plasma properties, including electron density, gas temperature, and plasma volume, the H_2O_2 production rate and energy yield, and the energy dissipation into the liquid were determined at different liquid conductivity. The energy dissipation into the bulk liquid increased as the liquid conductivity increased causing the total input energy to increase and resulting in a small decrease in H_2O_2 energy yield. In addition, the production rate of H_2O_2 didn't change significantly with conductivity for the helium plasma but decreased about 13 percent in the argon plasma. The energy deposited in the helium plasma didn't change with conductivity, thereby causing the H_2O_2 energy yield based upon energy in the plasma to be constant with conductivity. A model based upon the electrical circuit was used to predict the breakdown voltage for a range of liquid conductivity up to 36 mS/cm. This model also showed that decreasing the rise time of the applied voltage (i.e., faster rising rate) significantly increased the breakdown voltage, and therefore improved the liquid conductivity tolerance of the plasma system allowing it to function at near sea-water conductivity.

KEYWORDS: nanosecond pulsed plasma, H_2O_2 production, liquid conductivity, electrical breakdown, gas-liquid plasma

Introduction

Non-thermal plasma technology has been widely studied for water treatment since electrical discharges formed with liquid water generate reactive species such as hydrogen peroxide (H_2O_2) and hydroxyl radicals (·OH), and these reactive species can degrade pollutants in the liquid phase into partially oxidized or completely mineralized products [1-4]. Because it is based upon these highly reactive species, non-thermal plasma technology, also considered a type of Advanced Oxidation Process [5], has a much faster treatment time than conventional biological methods, and it can also degrade organic compounds which are difficult to degrade by microorganisms [4, 6]. The influence of operating conditions such as the reactor geometry, power supply characteristics and plasma properties, and liquid flow rate on the wastewater treatment efficiency and the yield of various reaction products was investigated in previous studies [7-10].

The effects of liquid conductivity were also studied in the previous work since many contaminated sources of water, including various drinking water and industrial waste water, can have a very high liquid conductivity, and many plasma processes where the plasma discharge contacts liquid water are sensitive to the solution conductivity. The effects of conductivity on the chemical and physical processes in electrical discharges have been studied in cases of completely submerged underwater discharges. For example, Shih et al. [11] investigated the influence of liquid conductivity on the intensity of ·OH emission and the H_2O_2 generation rate of a microsecond pulsed discharge generated directly in the liquid phase. The ·OH emission and H_2O_2 generation rate decreased approximately 5 and 4 times, respectively, as the liquid conductivity was increased from 0.005 mS/cm to 1 mS/cm. Lukes et al. [12] reported that the UV emission increased 10 times but the H_2O_2 concentration decreased 6 times in the microsecond pulsed corona discharge generated directly in the liquid as the liquid conductivity was increased from 0.1 mS/cm to 0.5 mS/cm. They concluded that the decrease of H_2O_2 yield was due to increasing rates of photolysis as liquid conductivity was increased. Maehara et al. [13] found that the ·OH concentration decreased and then increased as the liquid conductivity was increased from 0.002 mS/cm to 70 mS/cm in an RF plasma generated directly in the liquid.

The effects of liquid conductivity on discharges generated over and in contact with liquid surfaces, including bubbles and aerosol droplets, have also been studied. Kornev et al. [14] investigated the influence of liquid conductivity on the energy dissipation and the stability of a nanosecond pulsed corona discharge. In their study, the plasma was generated between two parallel plate electrodes, and water droplets were sprayed into the discharge zone. They found that the energy dissipation into the treated solution reached 30 percent of the delivered energy to the reactor when increasing the liquid conductivity to 45 mS/cm, and the transition of a corona discharge to a spark discharge took place at this high liquid conductivity. Hamdan et al. [15] reported the effects of liquid conductivity on the discharge characteristics of nanosecond pulsed spark discharges generated inside gas bubbles immersed in a liquid. They found that the discharge probability, which they defined as the number of successful discharge out of 200 pulses, decreased from 50% to less than 5% and the plasma volume decreased about 5 times upon increasing the liquid conductivity from 0.01 mS/cm to 2.00 mS/cm. However, the electron density did not change significantly with the liquid conductivity. Midi et al. [16] studied how water conductivity affected the discharge emission

and the current distribution in a microsecond pulsed spark discharge generated on the surface of a liquid, and they concluded that the liquid conductivity influenced the electric field and therefore affected the current distribution. Akishev et al. [17] studied the influence of liquid conductivity on positive gas phase streamers propagating on the surface of bubbles and foams, and they concluded that the conductivity of the liquid decreased the strength of the electric field at the head of the streamer, thus affecting the electric breakdown.

In general, the effects of liquid conductivity on the light emission, product yield, energy dissipation, and discharge probability were studied for different plasma systems. However, few studies discussed the effects of liquid conductivity on the formation of plasma and electrical breakdown. Yan et al. [18] investigated the effects of liquid conductivity, applied voltage, and electrode diameter on the generation of microsecond pulsed plasma inside liquid water using a computational model to simulate the formation of vapor layer on the electrodes during the pre-breakdown process. Their model showed that the plasma was formed faster at the high applied voltage in the highly conductive liquid using electrodes of small diameter. But they did not report how liquid conductivity affects the breakdown voltage. Since the electrical breakdown is the key step for generating plasma discharge, it is therefore very important to determine how the liquid conductivity influences the breakdown in order to improve the liquid conductivity tolerance of plasma systems. The liquid conductivity tolerance, which we term here the maximum liquid conductivity where electrical breakdown occurs and a plasma discharge is formed, is usually related to the nature of the power supply as well as the geometry of the reactor and the means of contacting the plasma with the liquid. In our previous work [9, 19], an ignition coil was combined with a function generator to produce microsecond pulsed discharges in a small water film plasma reactor [20]. This type of power supply generates pulses with relatively long rise time (about 4 μs) and pulse width (>100 μs). With this power supply no discharge was generated when liquid conductivity was higher than 0.5 mS/cm.

According to Zhang et al. [21] the breakdown voltage is negatively related with the pulse rise time in a gas phase dielectric barrier discharge. Komuro et al. [22] and Huiskamp et al. [23] showed that shorter voltage rise times made the emission of streamer discharge generated in air stronger and the propagation rate of streamer head faster than streamers generated by applying voltages with longer rise times. Therefore, in the present work we used a fast-rising nanosecond pulsed power supply with a water film gas-liquid plasma reactor to investigate the system performance over a wider range of liquid conductivity. The liquid conductivity was adjusted by adding KCl to deionized (DI) water, and the plasma properties including electron density, gas temperature and plasma volume, H_2O_2 production rate and energy yield, and discharge energy were measured. The influence of liquid conductivity on the breakdown voltage was also investigated through experiments and an electrical circuit simulation. The results showed that the fast rise time and short pulse system has a much higher liquid conductivity tolerance and can generate a strong discharge even when the liquid conductivity is as high as 36 mS/cm.

Methods

Experimental setup

The same water film plasma reactor and experimental setup, Figure 1 (a), were used as in previous studies [7, 24, 25]. As shown in Figure 1 (b), the liquid and gas mixture entered the reactor through the upper nozzle and exits the reactor through the lower nozzle. A water film along the reactor wall was formed as soon as the liquid-gas mixture enters the reactor due to the high pressure of the carrier gas (approximately equal to 200 kPa). The pressure of the mixture inside the reactor was estimated to be 2.5 atm using choked flow theory [26]. The upper and

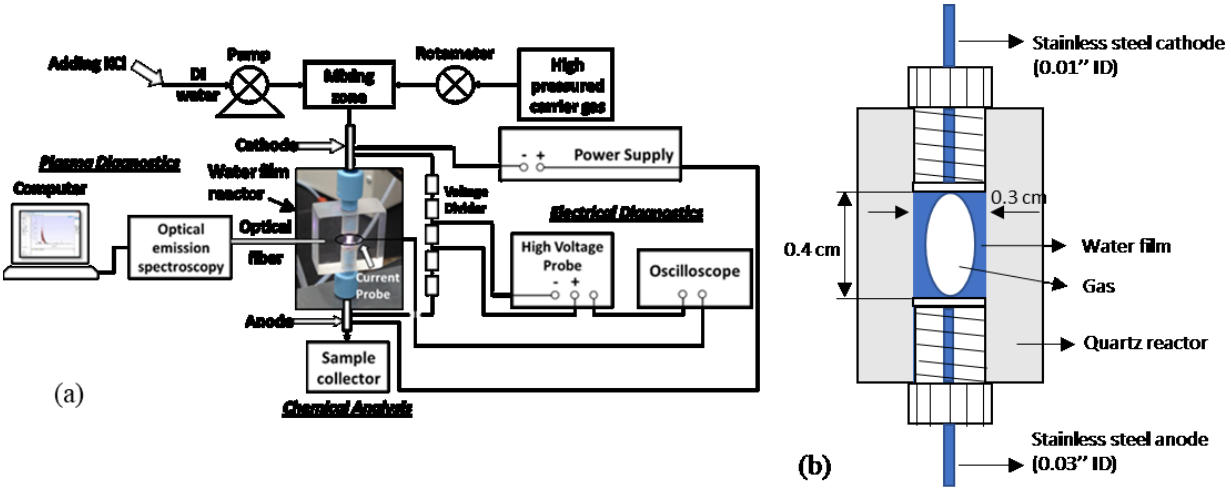

Fig 1. (a) Experimental set up and (b) the sketch of water film plasma reactor

lower nozzles also function as the cathode and anode, respectively, and were connected to a nanosecond pulsed power supply (NSP 120-20, Eagle Harbor Technologies, LLC, Seattle Washington) to generate the non-thermal plasma along the surface of the water film. The liquid sample flowing out of the reactor was collected, and the concentration of H_2O_2 in the liquid samples was measured [9, 26-28] by adding titanium sulfonate and measuring the absorption of light at 407 nm through the sample with a UV-Vis spectrometer (Perkin-Elmer, Lambda 35; Waltham, MA). Since the water-film reactor is a continuous flow steady-state reactor, the concentration of H_2O_2 in the liquid sample is not affected by the sample collection time. The average production rate of H_2O_2 was calculated by multiplying the H_2O_2 concentration by the liquid flow rate. The residence time of the liquid in the reactor is 150 ms, therefore the production rate of H_2O_2 represents the production of H_2O_2 averaged over many pulses. Plasma diagnostics were conducted using an optical emission spectroscopy (Avantes, AvaSpec-ULS3848) with a resolution of 0.13 nm to measure the plasma properties including electron density and gas temperature. Electrical diagnosis was performed using a Rogowski coil (Pearson Electronics, model 6585; Palo Alto, CA) and a high voltage differential probe (Tektronix, THDP0100) with 75 MHz bandwidth. The Rogowski coil was placed around the discharge region of the plasma to directly measure the discharge current [7]. A resistor chain of 5000 Ω was connected in parallel with the reactor to function as the voltage divider, and the high voltage probe was connected to

one of the resistors in order to protect the probe from being damaged by the high voltage pulses. Both the Rogowski coil and the high voltage probe were connected to an oscilloscope (Tekronix MDO 3014; Beaverton, OR) to display and record both the voltage and current waveforms. The total energy consumed in each pulse was calculated with equation (1).

$$\mathrm{E_{tot}} = \int V_{exp}(t) I_{exp}(t) dt \tag{1}$$

Where V_{exp} and I_{exp} are the total discharge voltage and current measured from the experiment. The overall energy yield of H_2O_2 was calculated by dividing the production rate of H_2O_2 (in grams/s) by the total consumed power (in watts).

Gas temperature measurement using OH(A-X) peak

The same two-temperature fitting method was used as in our previous work [7] since the abundance of water in the system makes the rotational distribution of ·OH deviate from the Boltzmann distribution [29, 30]. To use the two-temperature fitting method, the Boltzmann plot was generated using MassiveOES [31-33] as shown in Figure 2, and the plot was fitted to minimize the expression given in equation (2).

$$\min_{(a_1, a_2, T_1, T_2)} \Sigma_{(J',N')} \left[\ln\left(a_1 e^{-E_{(J',N')}/(kT_1)} + a_2 e^{-E_{(J',N')}/(kT_2)} \right) - \ln\left(\frac{n_{(J',N')}}{2J'+1} \right) \right]^2 \tag{2}$$

Where a_1 and a_2 are the linear factors for the cold and hot groups, and the T_1 and T_2 are the temperatures corresponding to the cold and hot groups respectively. The temperature of the cold

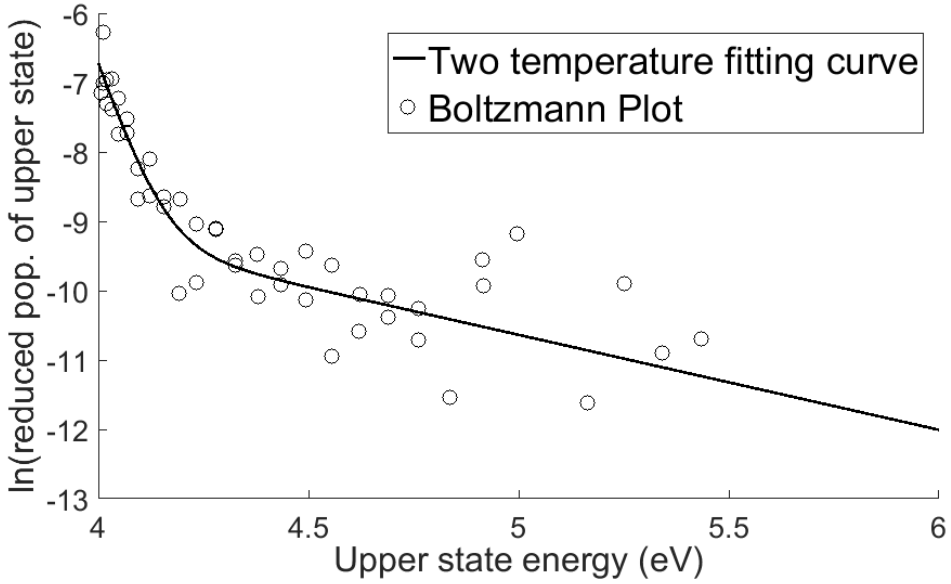

Fig 2. Boltzmann plot and two temperature fitting curve of OH (A-X) peak in helium plasma generated in DI water at 20 kV, 50 ns, and 2 kHz. The liquid flow rate is 1 mL/min.

group was found to be close to the gas temperature of the plasma [31]. Three Boltzmann plots

were generated using MassiveOES for each spectrum, and the temperature measurement was repeated three times for each condition. The error bars for the gas temperature are based upon one standard deviation. For the spectrum of the plasma generated in argon as shown in Figure 3 (a), the 'baseline' of the spectrum was determined and subtracted before generating the

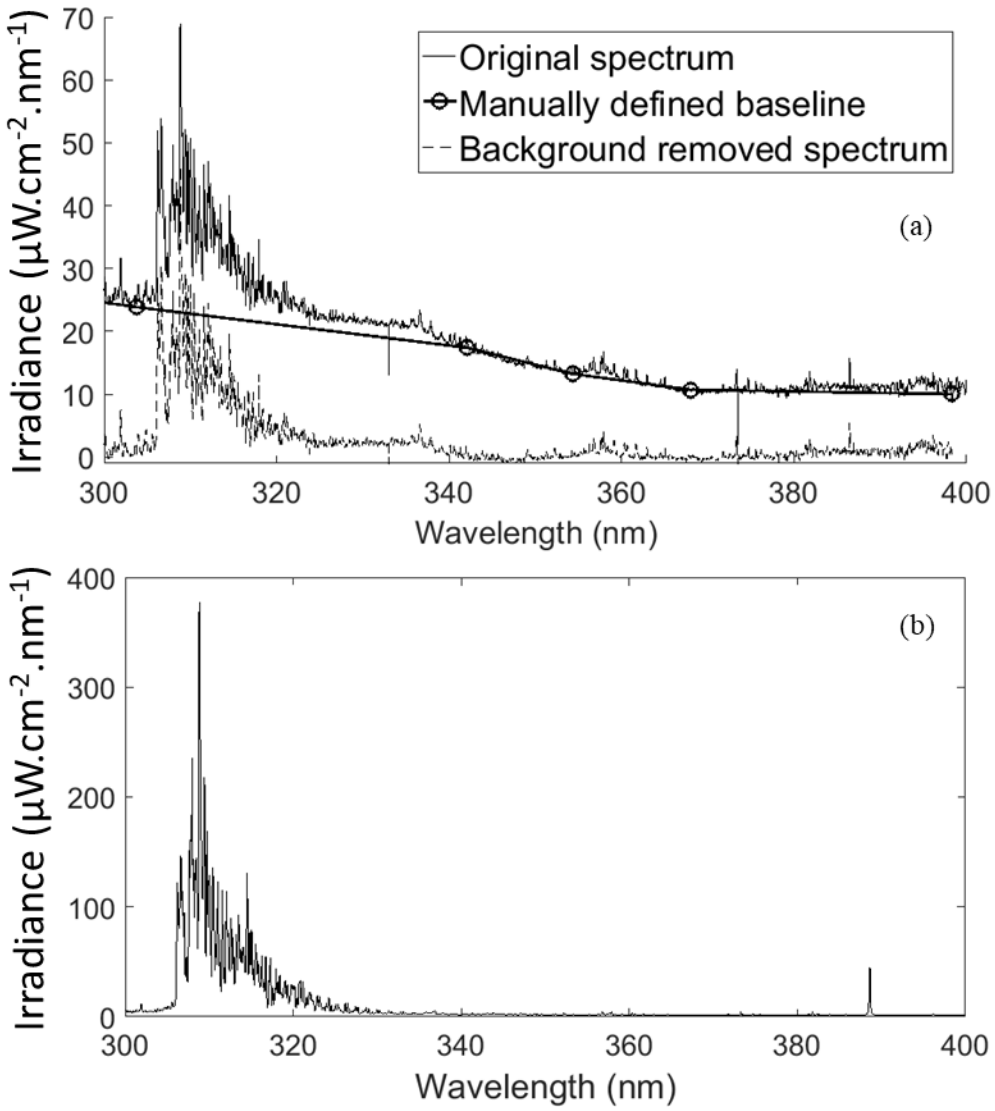

Fig 3. Spectrum in the 300-400 wavelength range of (a) argon discharge and (b) helium discharge. The power setting was fixed at 20kV, 50ns, and 2kHz. The liquid flow rate is 1 mL/min, and DI water was used in this case.

Boltzmann plot since the intensity of the continuum radiation is very strong. The strong intensity of the continuum spectrum in the argon plasma is possibly caused by the higher electron density of argon plasma since the continuum spectrum is directly influenced by the electron density [34]. Variation in subtracting the spectrum baseline causes significant differences among the Boltzmann plots, and this leads to the larger error bars in the gas temperature measurement of the argon plasma. The baseline removal is not necessary for the helium plasma since the continuum radiation is

relatively weak as shown in Figure 3 (b). Therefore, the error bars for the gas temperature of helium plasma are small.

Electron density measurement

The electron density of the helium discharge was measured using the Stark broadening of the H_α peak. The peak was first deconvoluted into the Gaussian and Lorentz profiles by fitting the overall peak profile to the Voigt function [35].

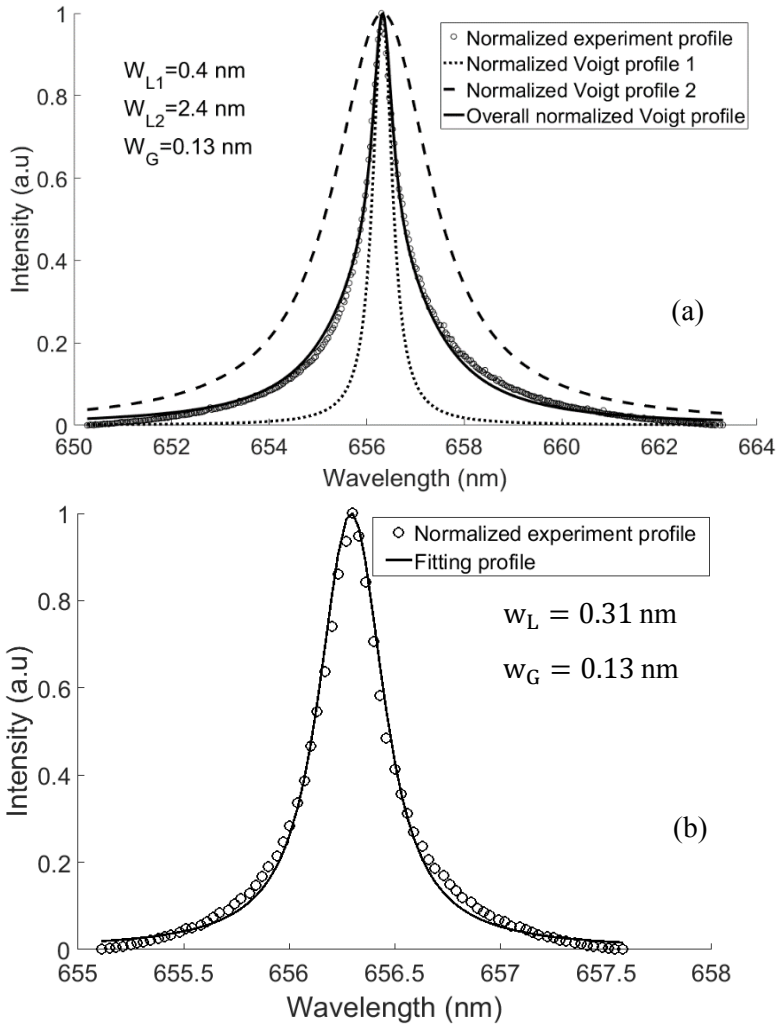

Fig 4. (a) H_α peak fitting in argon discharge and (b) H_α peak fitting in helium discharge. The power setting was fixed at 20 kV, 50 ns, and 2 kHz. The liquid flow rate is 1 mL/min, and DI water was

The Gaussian profile was determined by the Doppler and instrument broadening. The FWHM of instrument Broadening was determined by the resolution of the OES, and the FWHM of the Doppler broadening was calculated with equation (3) [35].

$$w_D = 7.162 \times 10^{-7} w_c \sqrt{\frac{T_g}{M}} \quad (3)$$

Where T_g is the gas temperature, measured using the OH (A-X) peak from the experiment, w_c is the wavelength of the center of the peak, and M is the atomic mass of the emitter. The FWHM of the Gaussian profile (w_G) was determined by equation (4) [35].

$$w_G = \sqrt{w_D^2 + w_{in}^2} \quad (4)$$

Where w_{in} is the FWHM of instrument Broadening. This allows to fix the Gaussian part of the Voigt profile which makes the fitting procedure more robust. The Van der Waals and Stark Broadening contribute to the Lorentz profile. The FWHM of Van der Waals Broadening was calculated by equation (5) [35].

$$w_{\mathrm{vdw}} = \frac{C}{T_g^{\frac{7}{10}}} \quad (5)$$

Where T_g is the gas temperature of plasma, C is the constant determined by what type of carrier gas was used, and its value equals to 5.12 and 2.42 respectively [36] for argon and helium, respectively. The FWHM of Stark broadening was calculated by subtracting the FWHM of the Van der Waals broadening from the FWHM of the Voigt profile as given by equation (6) [35].

$$w_s = w_L - w_{vdw} \quad (6)$$

The electron density was then calculated using equation (7) [35].

$$\mathrm{w_S} = 1.78\ \mathrm{nm} \times \left(\frac{n_e}{10^{23} m^{-3}}\right)^{0.67965} \quad (7)$$

Where $\mathrm{w_S}$ is the FWHM of Stark broadening, n_e is the electron density.

The argon discharge is highly inhomogeneous[37, 38], especially when the discharge power is high. Therefore, fitting the H_α peak using a single Voigt function is difficult in an argon plasma. To take the inhomogeneity into consideration, the profile of H_α in the argon discharge was fitted to a combination of two Voigt functions, as in equation (8), corresponding to the high and low electron densities, respectively.

$$a f_{v,1}(x; w_{G1}, w_{L1}) + (1 - a) f_{v,2}(x; w_{G2}, w_{L2}) \quad (8)$$

Where a is the coefficient defining the contribution of Voigt profile 1 to the overall peak profile. The average electron density was calculated by equation (9).

$$n_e = a n_{e1} + (1 - a) n_{e2} \quad (9)$$

Where n_{e1} and n_{e2} are the electron densities calculated using the FWHM of the Lorentz profile (w_{L1} and w_{L2}) in equation (8), respectively.

The H_α peak in both argon and helium plasma was automatically fit to the equations using the FIT function in MATLAB, and the fitting profile is shown in Figure 4. The measurement of electron density was repeated three times, and the error bar was set to one standard deviation for each condition.

Estimation of cross-sectional area of plasma channels

Since a filamentary discharge is formed in the water film plasma reactor as shown in Figure 5, and the volume of the plasma is difficult to determine from the photographic images, the current density was used to estimate the volume of the plasma and the contact area between the liquid and plasma by equation (10) [7, 35].

$$A = \frac{I_{g,max}}{J} = \frac{I_{g,max}}{n_e e \mu_e E} \quad (10)$$

Where A is the cross-sectional area of a plasma channel, $I_{g,max}$ is the peak discharge current determined by subtracting the current which passes through the liquid film from the total discharge current measured in the experiment, J is the current density of the plasma, e is the

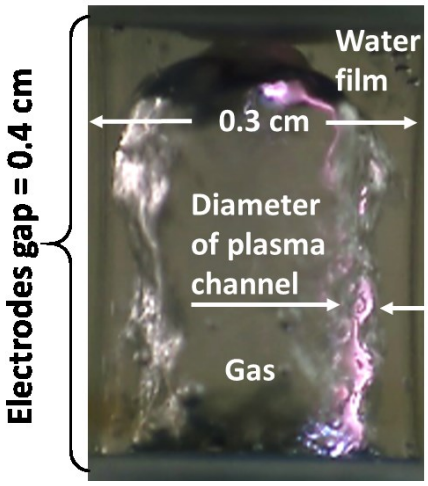

Fig 5. Zoomed in photo of the discharge region and filamentary plasma channel formed along the surface of the water film for the argon carrier gas.

elementary charge, μ_e is the mobility of electrons estimated using Bolsig+ (version 03/2016) [39], n_e is the measured electron density, and E is the electric field estimated using the discharge voltage and the electrode gap distance. In addition, since the peak discharge current and the electron density were measured using the time and spatially averaged spectra, the cross-sectional area estimated using equation (10) is close to the maximum cross-sectional area of the plasma channel during one pulse. The maximum contact area between the plasma and liquid was estimated by assuming that the plasma channel is cylindrical and only half of the plasma contacts the liquid as in equation (11).

$$\text{Area} = \pi r_p l \tag{11}$$

Where l is the length of the plasma channels, approximately equal to the length of the reactor which is the same as the electrode gap distance, and r_p is the radius of the plasma channel.

Simulation of discharge voltage and current using current balance equation

A model based upon the electrical circuit shown in Figure 6 (a) was developed to study how liquid conductivity influenced the electrical breakdown. The model was constructed based on the current pathway as shown in Figure 6 (b). The total current of the circuit equals the displacement current added to the conductive current as shown by equation (12) [40, 41].

$$I_o = I_{con} + I_{dis} \tag{12}$$

Where I_o, I_{con}, and I_{dis} represent the total current passes the plasma system, conductive current, and displacement current, respectively. The displacement current is caused by the capacitance of the reactor, and the conductive current includes the current passing through the plasma channel, water film, and the voltage divider. The current was assumed to not flow across the interface between the plasma and liquid since the plasma is much more conductive compared with the liquid. The conductive current is dependent on the resistance of the voltage divider, liquid film, and plasma channel. The conductivity of plasma can be given by $\sigma_p = e\mu_e n_e$ [35, 42].

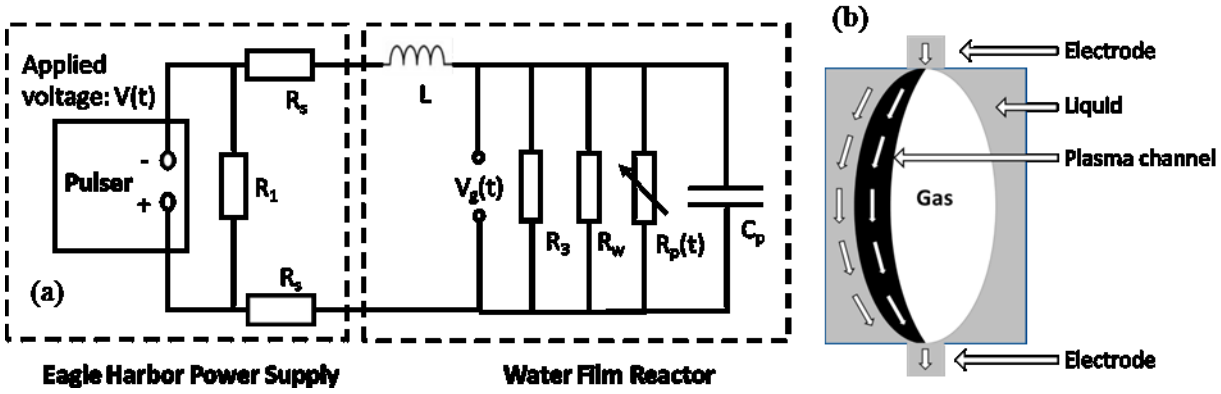

Fig 6. (a) Description of the circuit for simulating the plasma discharge in the water film plasma reactor. (b) Current flow pathway in water film plasma reactor assuming the liquid is conductive.

Therefore, the resistance of the plasma channel (R_p) can be estimated using equation (13). The resistance of plasma is a function of time, and its value at a specific time point is inversely proportional to the electron density [21, 43] as shown in equation (13).

$$R_p \approx \frac{l}{A\sigma_p} = \frac{l}{Ae\mu_e n_e(t)} \tag{13}$$

A is the cross-section area of plasma channel, and it changes with time during a single pulse. But since the change of A is not as significant as electron density, the maximum cross section area

estimated using equation (10) was used and was assumed to be the constant in the model. Therefore, the total current in equation (12) can be written as in equation (14).

$$I_o(t) = C_p \frac{dV_g(t)}{dt} + \frac{V_g(t)}{R_p(t)} + \frac{V_g(t)}{R_w} + \frac{V_g(t)}{R_3} \tag{14}$$

C_p is the measured capacitance of the reactor, V_g is the discharge voltage of the plasma, and R_w and R_3 are the resistance of the liquid film and the voltage divider, respectively.

The total voltage in the circuit is given by equation (15).

$$V(t) = 2R_s I_o(t) + V_g(t) + L\frac{dI_o}{dt} \tag{15}$$

$V(t)$ is the applied voltage, L is the stray inductance of the wires, and R_1 and R_s are the resistances as shown in Figure 6 (a). The applied voltage is determined by the power supply and was assumed to not be affected by the outer circuit. Combing equation (14) and equation (15), gives equation (16).

$$V(t) = LC_p \frac{d^2V_g}{dt^2} + \left(2C_pR_s + \frac{L}{R_w} + \frac{L}{R_3}\right)\frac{dV_g}{dt} + L\frac{d}{dt}\left(\frac{V_g(t)}{R_p(t)}\right) + \left[\frac{2R_s}{R_p(t)} + \frac{2R_s}{R_w} + \frac{2R_s}{R_3} + 1\right]V_g(t) \tag{16}$$

At the beginning of the pulse, the discharge voltage and the rate of rise of the discharge voltage equal zero. Therefore, the initial conditions for equation (16) can be given by equations (17) and (18).

$$V_g(t=0) = 0 \tag{17}$$

$$\left.\frac{dV_g}{dt}\right|_{t=0} = 0 \tag{18}$$

According to Simeni et al. [44], the time resolved electron density of a nanosecond pulse discharge over the surface of liquid water increased and decayed rapidly with discharge current. Due to the limitation of the instrument, the time-resolved electron density of current work cannot

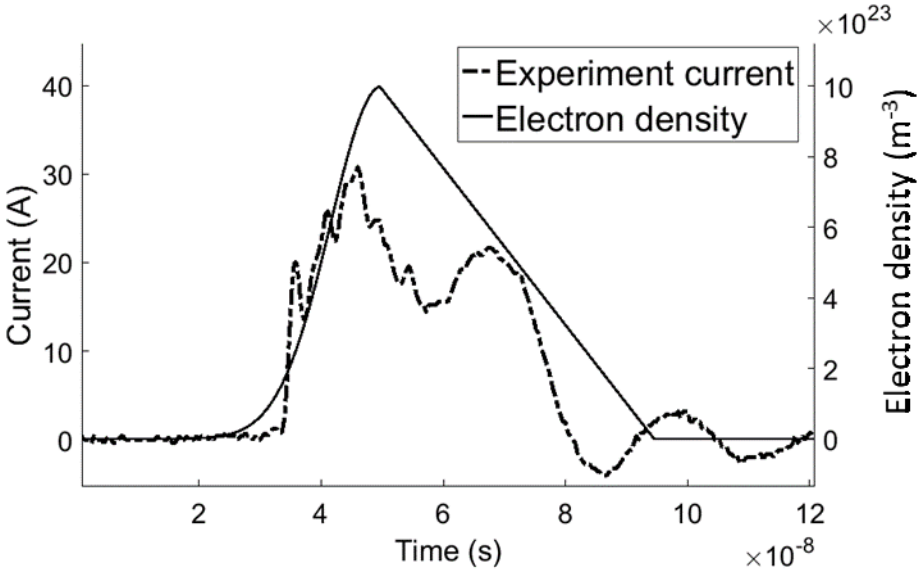

Fig 7. Assumed electron density variation with time in the argon plasma.

be measured from the experiment. Therefore, the electron density in our work was assumed to exponentially increased from 0 to 10^{24} m^{-3} and then linearly decay simultaneously with the discharge current in the argon plasma as shown in Figure 7. The electron density measured from the experiment using the time average spectrum is on the order of magnitude of 10^{23} m^{-3}, therefore we assumed the maximum electron density to be 10^{24} since we expected the maximum electron density during one pulse to be larger than the electron density measured using the time and spatially averaged spectrum. The rise time of the applied voltage is about 20 ns according to the power supply manufacturer's specifications. The applied voltage function was defined by equation (19).

$$V(t) = \begin{cases} 0 & (t < 10\ ns) \\ \frac{V_p}{20\times10^{-9}}(t - 10^{-9}) & (t > 10\ ns\ and\ t < 30\ ns) \\ V_p & (t > 30\ ns\ and\ t < 60\ ns) \\ V_p - \frac{V_p}{20\times10^{-9}}(t - 60\times10^{-9}) & (t > 60\ ns\ and\ t < 80\ ns) \\ 0 & (t > 80\ ns) \end{cases} \quad (19)$$

V_p is the peak value of the applied voltage, equal to the 20 kV constant input voltage.

By using the two initial conditions, (17) and (18), and the equations that describe the change of electron density (shown in Figure 7) and the applied voltage, equation (16) was solved using MATLAB to determine the discharge voltage. The discharge current was then calculated using equation (20).

$$\mathrm{I_g(t)} = \mathrm{V_g}(t)/R_p(t) \quad (20)$$

Estimation of energy dissipation in the liquid

The capacitance of the plasma reactor which is related to the geometry of the plasma reactor was estimated from the displacement current using equation (21). The applied voltage, pulse width and frequency were set to 200V, 20 ns and 1000 Hz, respectively, to avoid electrical breakdown. The voltage change was measured using a high voltage probe, and the displacement current was measured using a Rogowski coil placed around an HV lead.

$$\mathrm{I_{dis}} = \mathrm{C_p}\frac{dV}{dt} \quad (21)$$

The resistance of the liquid film was estimated using a similar method by placing the Rogowski coil centered on the reactor at the discharge region, and when there is no discharge generated, the measurement captures current passing through the liquid film. The resistance of the water film at different liquid conductivity was then determined by dividing the measured voltage by the measured current. Both the capacitance and resistance measurements were repeated three times, and the average value was determined and used in the circuit model. The stray inductance of the

wires in the circuit (L in Figure 6) was measured using an LCR meter (Agilent U1731C) by removing the HV lead from the output of the power supply.

The energy dissipated in the liquid was determined using equation (22) with equation (23).

$$\mathrm{E_{dissipation}} = \int I_w(t) V_{exp}(t)\, dt \tag{22}$$

$$\mathrm{I_w}(t) = \frac{V_{exp}(t)}{R_w} \tag{23}$$

$\mathrm{I_w}$ is the current passing through the liquid film during the plasma discharge, and it approximately equals zero when DI water was used.

Results and Discussion

Electrical diagnostics

Figure 8 shows the comparison of the current and voltage waveforms for discharges generated in DI water and 36 mS/cm KCl solutions. For the discharge in DI water, the current flow increased

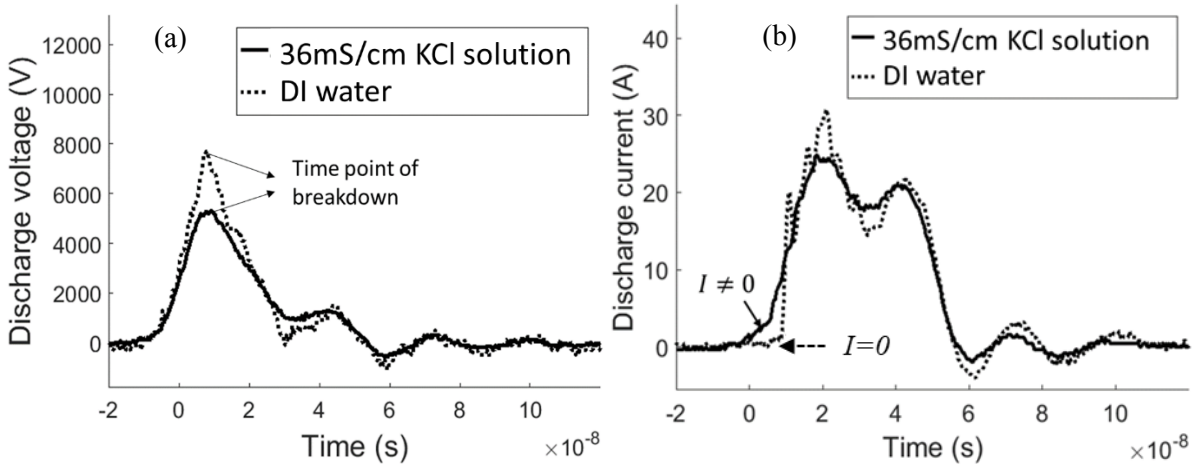

Fig 8. Waveform of (a) discharge voltage and (b) discharge current for argon plasma generated in DI water and 36 mS/cm KCl solution. The voltage setting, the pulse width, and the frequency of power supply were fixed at 20 kV, 50 ns, and 2 kHz, respectively. The liquid flow rate was set at 1 mL/min.

rapidly to its peak value as soon as the voltage reached the time point of breakdown, and the current flow was very small before the electrical breakdown since the DI water has a low conductivity. For the discharge in the highly conductive KCl solution, a significant amount of the current can pass through the liquid film before the electrical breakdown. Therefore, more of the energy was dissipated in the liquid, and the rate of current rise was relatively slower than for the case of low conductivity.

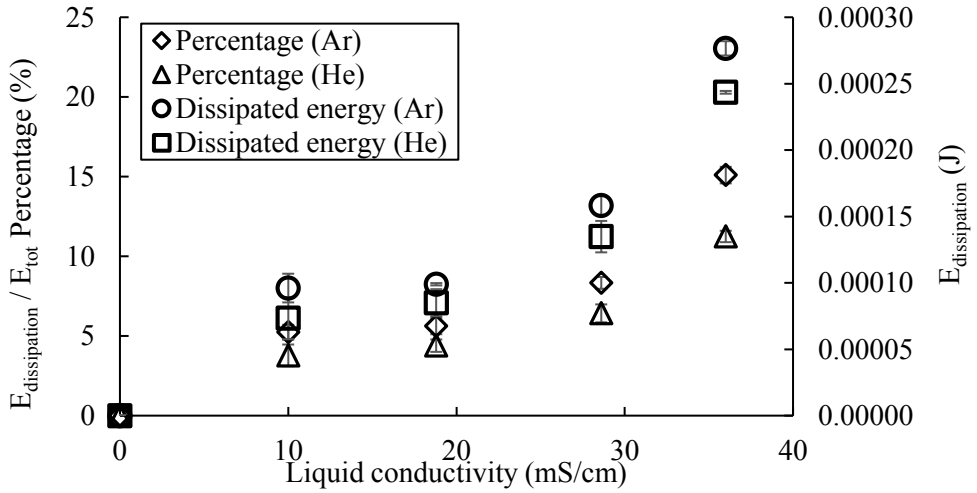

Fig 9. The change of $E_{dissipation}$ / E_{tot} Percentage and the energy dissipated in the liquid per pulse with different liquid conductivity. The voltage setting, the pulse width, and the frequency of the power supply were fixed at 20 kV, 50ns, and 2 kHz, respectively. The liquid flow rate was set to 1mL/min.

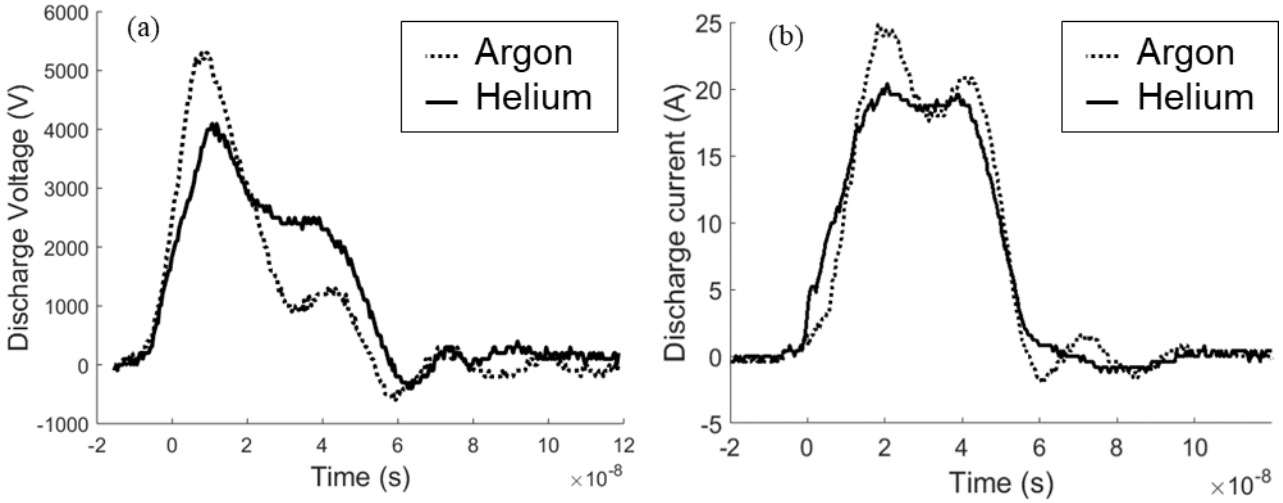

Fig 10. (a) The discharge voltage and (b) the discharge current waveform of argon and helium plasma generated in 36 mS/cm KCl solution. The voltage setting, the pulse width, and the frequency of power supplier were fixed at 20 kV, 50 ns, and 2 kHz, respectively. The liquid flow rate was set at 1 mL/min.

The total energy dissipated in the liquid and the percentage of the dissipated energy ($E_{dissipation}$) relative to the total input energy (E_{tot}) increased with the liquid conductivity for both the argon and helium discharges as shown in Figure 9. This is because the current flowing through the water film generates heat and causes energy dissipation into the bulk liquid. Therefore, the percentage of the discharge energy relative to the total input energy, given by $100\times(1 - E_{dissipation}/E_{tot})$, decreased with the liquid conductivity. The dissipated energy consumed about 10 and 15 percent of the total input energy in the helium and argon plasmas, respectively, at 36 mS/cm. However, according to the two-way ANOVA test described in the appendix, the energy

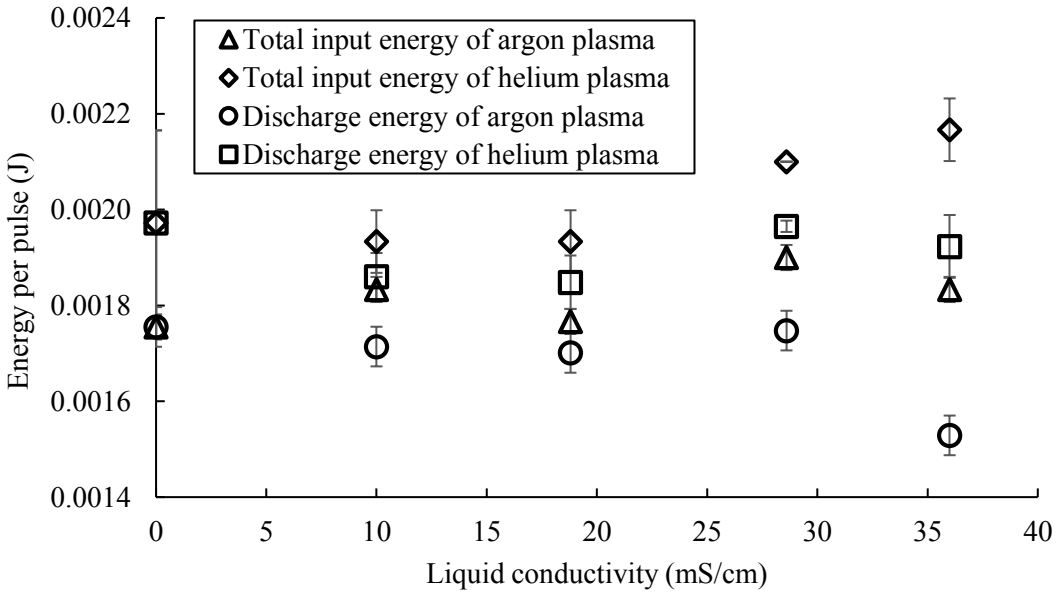

Fig 11. The total input energy and the discharge energy consumed by plasma as a function of liquid conductivity. The voltage setting, the pulse width, and the frequency of power supplier were fixed at 20 kV, 50ns, and 2 kHz, respectively. The liquid flow rate was set at 1mL/min.

dissipation doesn't change significantly with carrier gas. This is probably because the average discharge voltages for helium and argon, calculated by dividing the integral of the discharge voltage with time by the pulse duration, are not significantly different at each wavelength. As shown in Figure 10 (a), the waveform of the discharge voltage is similar in both the argon and helium plasmas. Therefore, the current flow through the water film determined using equation (23) is similar in both argon and helium plasmas, and the energy dissipation into the liquid is about the same at each liquid conductivity since the resistance of the liquid film is not affected by the carrier gas.

Figure 11 shows the total input energy and the discharge energy consumed by the plasma as functions of liquid conductivity. According to the result of the one-way ANOVA test described in the appendix, the influence of liquid conductivity on the total input energy per pulse was not statistically significant in both the argon and helium cases. However, the discharge energy consumed by the plasma decreased with liquid conductivity in the argon plasma but didn't change significantly in the helium plasma.

Plasma diagnostics

Figure 12 shows the gas temperature and electron density of the argon plasma as functions of liquid conductivity. The change of gas temperature with liquid conductivity was not statistically significant according to the ANOVA test, but the electron density increased with the liquid conductivity up to 28 mS/cm with a larger increase between 28 and 36 mS/cm in argon plasma. This is probably because the volume of the argon plasma decreased with the liquid conductivity especially between the data points of 28 and 36 mS/cm, which led to an increase in electron density. The decrease of plasma volume is probably caused by the faster compensation of space

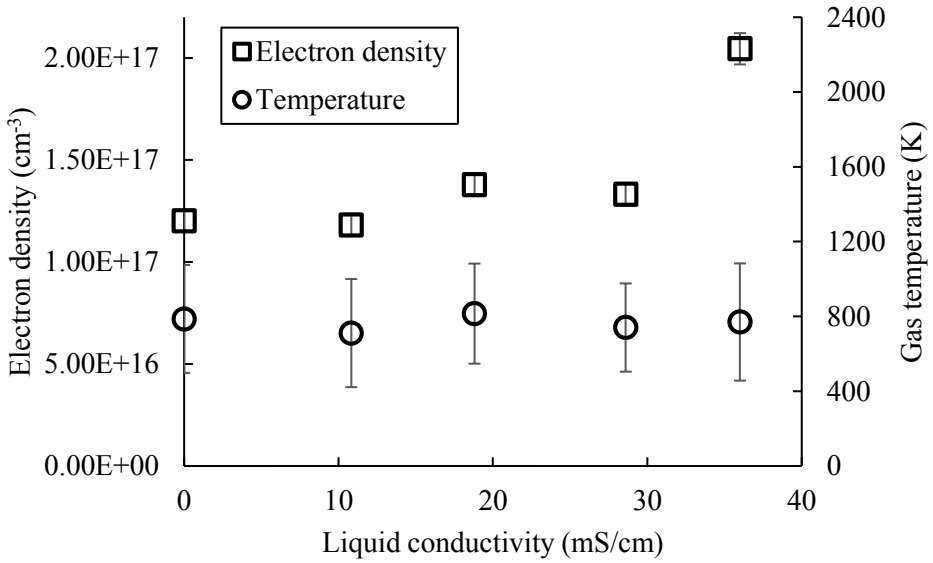

Fig 12. Gas temperature and electron density of the argon plasma as functions of the liquid conductivity. The voltage setting, the pulse width, and the frequency of power supplier were fixed at 20 kV, 50ns, and 2 kHz, respectively. The liquid flow rate was fixed at 1mL/min.

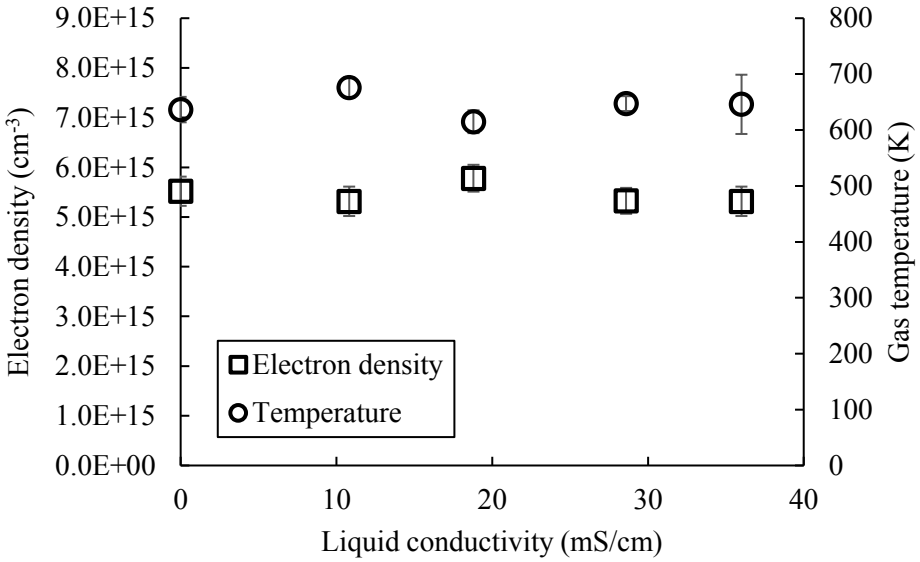

Fig 13. Gas temperature and electron density of helium plasma at different liquid conductivity. The voltage setting, the pulse width, and the frequency of power supplier were fixed at 20 kV, 50ns, and 2 kHz, respectively. The liquid flow rate was fixed at 1mL/min.

charge electric field on the streamer head [12, 17]. Sunka et al. [45] found that a denser but a cooler plasma with lower electron temperature was formed at the high liquid conductivity for an underwater discharge. However, Bruggeman et al. [46] reported the transition of a DC-excited under water discharge from the liquid mode to the bubble mode as the liquid conductivity was increased, and they found decreases in both electron density and electron temperature with the increasing liquid conductivity. Maehara et al. [13] reported that the electron density and excitation temperature were constant at 2.5 $\times 10^{20}$ m^{-3} and 4500 K, respectively in an RF

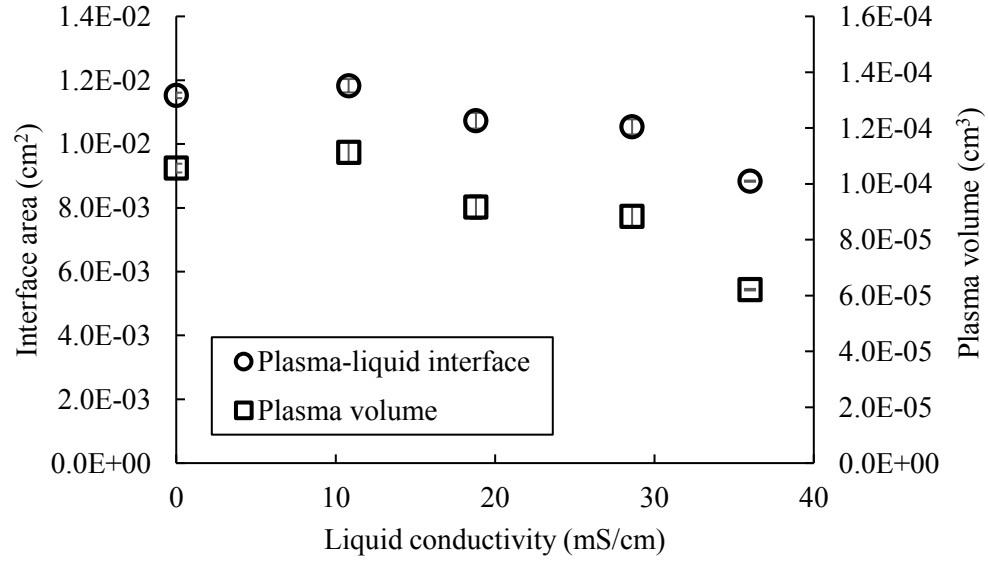

Fig 14. Plasma volume and area of plasma-liquid interface of argon plasma at different liquid conductivity. The voltage setting, the pulse width, and the frequency of power supplier were fixed at 20 kV, 50ns, and 2 kHz, respectively. The liquid flow rate was fixed at 1mL/min.

underwater plasma discharge as the liquid conductivity was increased from 0.002 mS/cm to 70 mS/cm. Hamdan et al. [15] also found that the electron density didn't change significantly with liquid conductivity in a nanosecond pulsed discharge formed in a bubble immersed in the liquid, a case which is perhaps more similar to our discharge than the direct underwater discharges.

Figure 13 shows that the electron density and gas temperature for the helium plasma were lower than those for the argon plasma and this is because a more diffuse plasma was generated in helium [7]. However, the gas temperature is about 2 times and the electron density is about 3 times higher in the present study than in our previous work with the same system [7]. This is probably because the discharge energy per pulse is about 3 times larger in the present study than in the previous study. Both the electron density and the gas temperature of the helium plasma didn't change significantly with liquid conductivity according to the ANOVA test.

Figure 14 shows the plasma volume and the area of the plasma-liquid interface of the argon plasma estimated by the current density model. The volume of the argon plasma decreased about 40 percent with increasing conductivity, and correspondingly the area of the interface between the plasma and liquid decreased about 20 percent. Figure 15 shows the volume and the area of the plasma-liquid interface of the helium plasma. The volume of the helium plasma is much larger than that of the argon plasma [7]. Further, the volume and the interface area of the helium

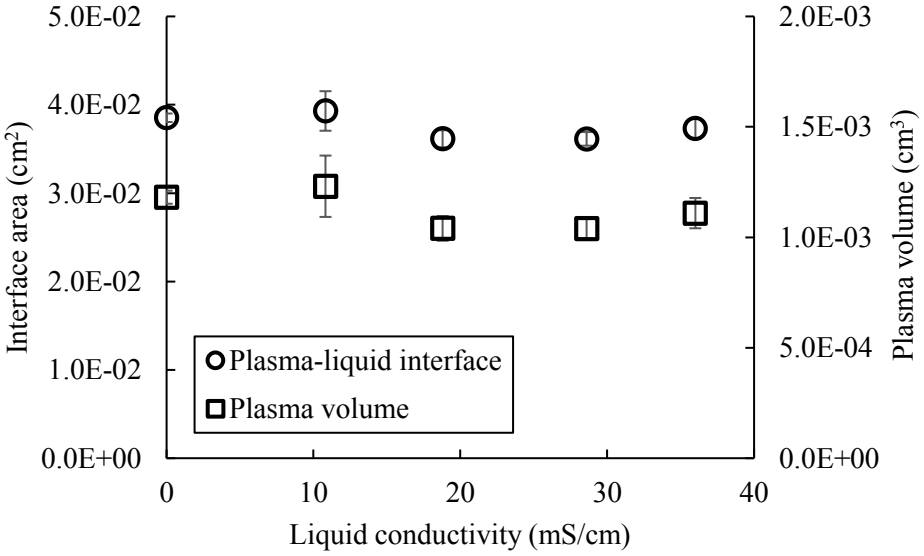

Fig 15. Plasma volume and area of plasma-liquid interface of helium plasma at different liquid conductivity. The voltage setting, the pulse width, and the frequency of power supplier were fixed at 20 kV, 50ns, and 2 kHz, respectively. The liquid flow rate was fixed at 1mL/min.

plasma didn't change significantly with the liquid conductivity according to the ANOVA test. The results in Figure 12 to Figure 15 are consistent with the results shown in Figure 11 in that the discharge energy consumed by the argon plasma decreased about 16 percent, but the energy consumed by helium plasma didn't change significantly as the liquid conductivity was increased from 0.01mS/cm to 36mS/cm. Therefore, the plasma properties of the helium plasma, including the electron density, gas temperature, and plasma volume, remain the same, but the plasma volume decreased and the electron density increased with the liquid conductivity in the argon plasma.

Future work is needed to determine what causes the different liquid conductivity effects in the argon and helium discharges.

H_2O_2 Production and concentration of ·OH

In previous work with a microsecond pulsed plasma system consisting of an ignition coil and a function generator [47], the H_2O_2 production rate dropped 62 percent in an argon discharge as the liquid conductivity was increased from 0.01 mS/cm to 0.3 mS/cm as shown in Figure 16 (a). Figure 16 (b) and the ANOVA tests, show that the production rate of H_2O_2 in the nanosecond pulsed plasma system decreased about 13 percent with liquid conductivity

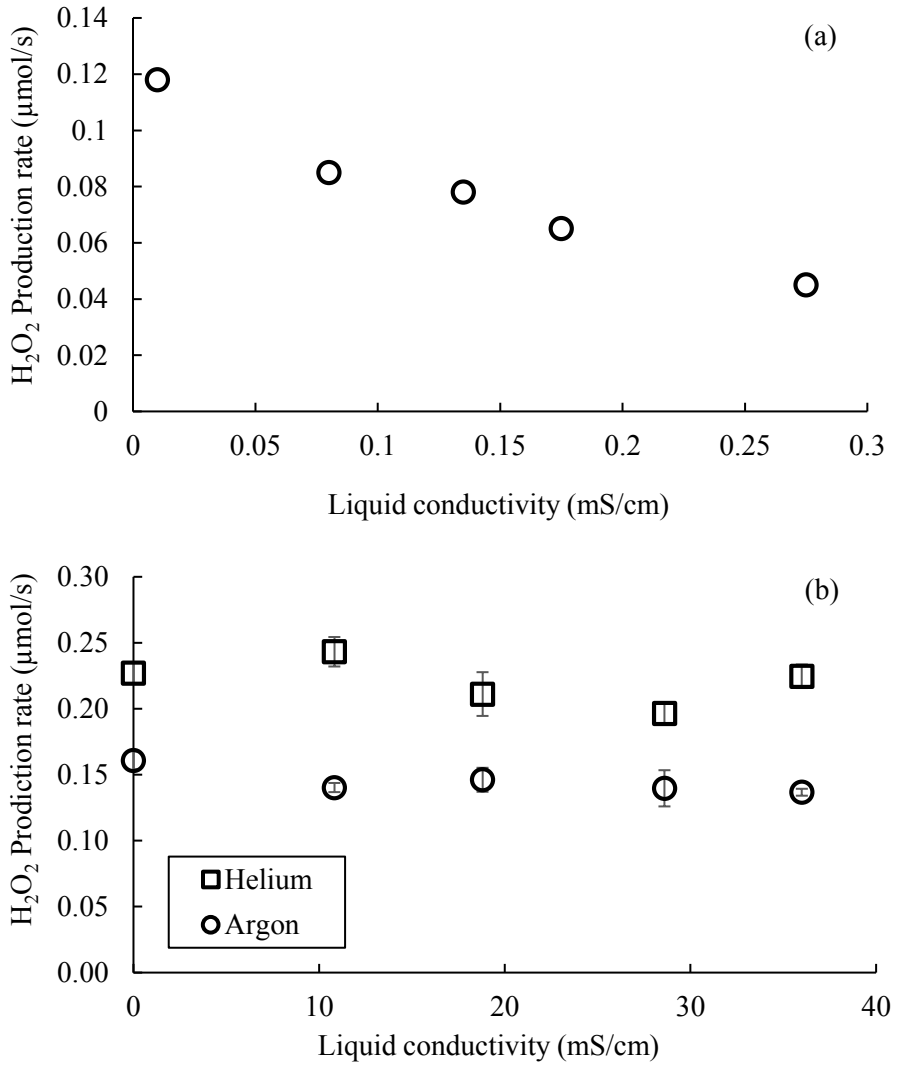

Fig 16. Production rate of H_2O_2 at different liquid conductivity for (a) the microsecond pulsed plasma system from reference [42] using argon as the carrier gas and (b) the nanosecond pulsed plasma system. The voltage setting, the pulse width, and the frequency of the nanosecond pulser were fixed at 20 kV, 50ns, and 2 kHz, respectively. The liquid flow rate was fixed at 1mL/min and 0.75 mL/min in nanosecond and microsecond pulsed plasma system, respectively.

over the full range from 0.01 mS/cm to 36 mS/cm in the argon plasma but didn't significantly change in the helium plasma. This suggests the nanosecond pulsed plasma system has a much higher liquid conductivity tolerance. The likely reason will be described in the following section.

According to our previous study [48], the H_2O_2 production rate is correlated with the area of the plasma-liquid interface since most of the H_2O_2 is formed in the film region near the interface. In addition, the H_2O_2 production rate is also affected by the electron density since the electron density influences the dissociation of water molecules, and therefore affects the formation of ·OH. The area of the plasma-liquid interface and the electron density of the helium plasma didn't change significantly with liquid conductivity as shown in Figure 13 and Figure 15. This explains the reason why the production rate of H_2O_2 in the helium discharge remained the same at different liquid conductivity. The plasma-liquid interface of the argon discharge decreased about 20 percent with liquid conductivity, which reduced the available volume for the recombination of ·OH. However, the increase of electron density in the argon discharge with liquid conductivity accelerated the dissociation of water molecules and generated more ·OH. Therefore, the effects of decreasing the plasma-liquid interface were partially cancelled out by the increasing electron density, and the H_2O_2 production rate only decreased 13 percent with liquid conductivity in argon plasma.

According to Figure 17 and the ANOVA test shown in the appendix, the overall energy yield of H_2O_2 decreased about 16% and 21% in the helium and argon discharges, respectively, as the liquid conductivity was increased from 0.01 to 36 mS/cm. The decrease of overall energy yield was caused by the energy dissipation through the liquid water as the liquid conductivity was increased. This is also shown by the unchanged energy yield of H_2O_2 based upon the discharge energy consumed by the plasma as shown in Figure 17. In general, the increase of liquid

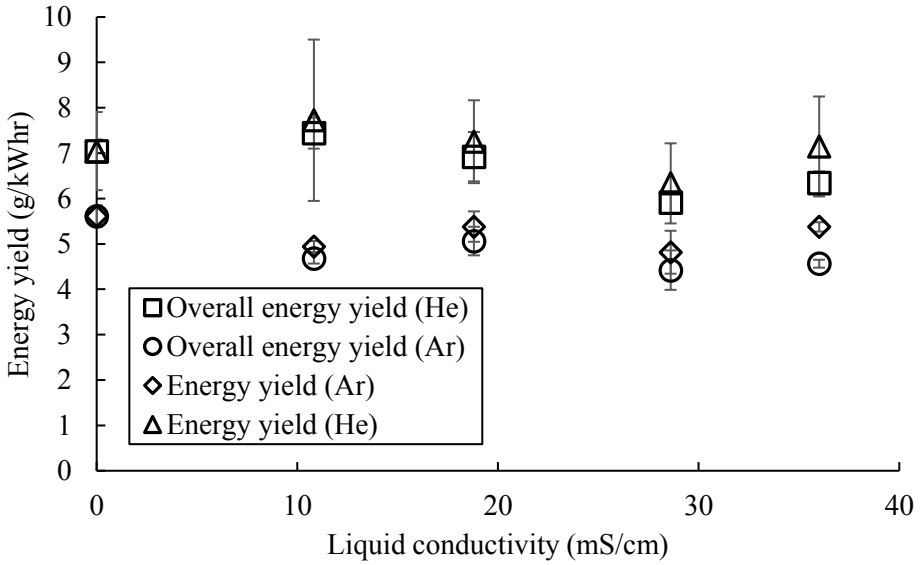

Fig 17. Overall energy yield and the energy yield of H_2O_2 calculated using the energy deposited in the plasma at different liquid conductivities. The voltage setting, the pulse width, and the frequency of power supplier were fixed at 20 kV, 50ns, and 2 kHz, respectively. The liquid flow rate was fixed at 1mL/min.

conductivity increased the current flow through the liquid which raised the energy dissipation into the liquid, but the energy consumed by the plasma discharge remained the same in the helium discharge and only decreased 17 percent in the argon discharge as shown in Figure 11. As a result, the overall energy yield decreased, but the energy yield calculated using the discharge energy consumed by the plasma remained the same with conductivity in both argon and helium plasma.

Figure 18 shows the average concentration of ·OH (<·OH >) estimated using a reaction model which was described in detail in our previous study [7]. Briefly, the model utilizes experimentally determined plasma properties including electron density, gas temperature, and plasma volume and H_2O_2 as inputs to determine the concentration of ·OH. This model was used in the present work to estimate the average concentration of ·OH for all the helium data points and the argon data points except at 36 mS/cm. At 36 mS/cm, the electron density of the argon plasma was about two times higher than the other argon plasma data points, which made the destruction of H_2O_2 by electrons in the model extremely fast. The rapid destruction rate made the concentration of H_2O_2 predicted by the model at this high conductivity small and the model could not be fit to the experimental result. This result suggests the need for further investigation of the argon plasma above 36 mS/cm.

According to Figure 18 and the ANOVA test, <·OH> decreased about 20 percent with the liquid conductivity increase from 0.01 to 28.6 mS/cm in the argon plasma but remained essentially the same in the helium plasma. The decrease of <·OH> and plasma volume resulted in the decrease

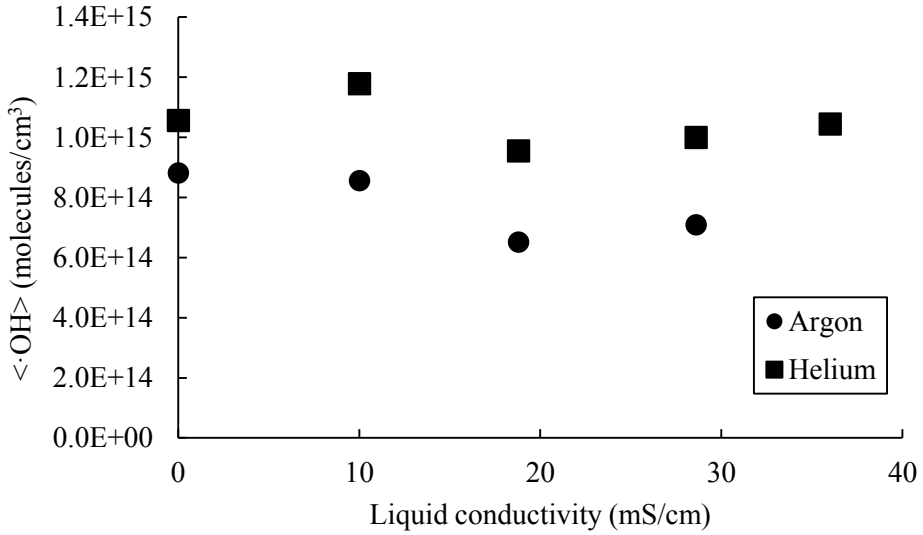

Fig 18. Average concentration of □OH (<·OH>) in the system predicted using the model described in [7] and the experimental results of electron density, plasma volume, and H_2O_2 concentration.

of H_2O_2 production rate in the argon plasma as shown in Figure 16. The decrease of the <·OH> in the argon plasma was probably due to the decrease in the discharge energy of the plasma with liquid conductivity as well as the slight change in plasma volume and electron density. This change of the <·OH> is consistent with the results in our previous study that showed lower discharge energy per pulse generated less ·OH [7]. The concentration of ·OH predicted by the model in the current study is about 2 and 4 times larger than in the previous study [7] for the argon and helium

discharges, respectively. This is probably because the input energy of the present study is about 3 to 4 times larger.

Circuit simulation of electrical breakdown

Figure 19 shows that the simulated discharge voltage and current are of the same order of magnitude as the experimental data, and the breakdown voltage predicted by the model compared well to the experimental result. Figure 20 shows the comparison of the breakdown voltage predicted by the model and the breakdown voltage measured from the experiment for the full range of conductivities. The predicted breakdown voltage fits the experimental breakdown

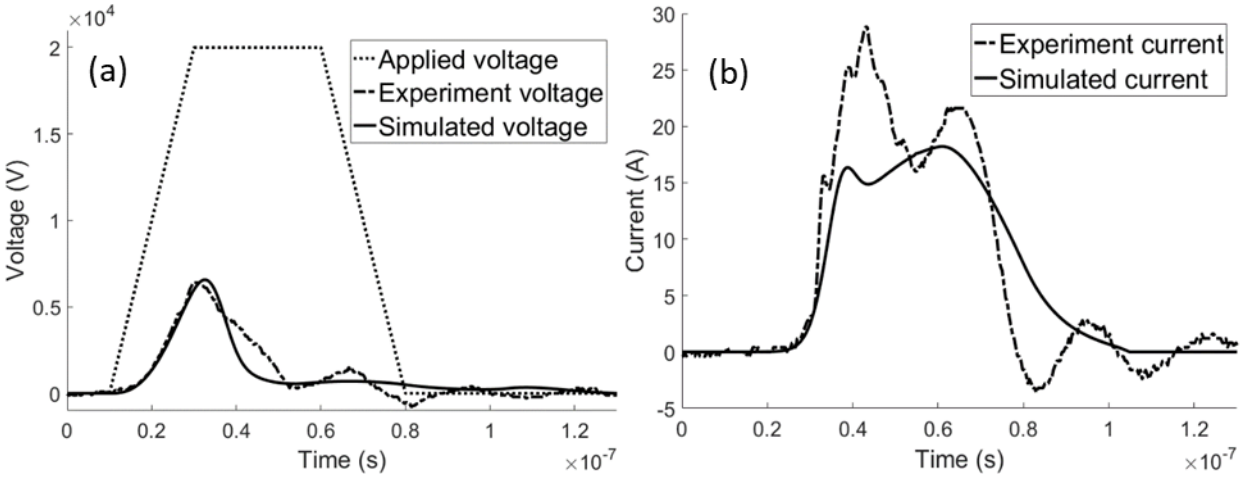

Fig 19. Comparison between (a) simulated discharge voltage and experimental discharge voltage; (b) simulated current and experiment current. The peak value of applied voltage was set to 20 kV, and the pulse width was set to 50 ns in the simulation. Argon was used as the carrier gas.

voltage quite well at the data points of 10 mS/cm, 18 mS/cm, and 28 mS/cm, and the slight lower breakdown voltages predicted by the model at the two extreme conductivities (0.01 and 36 mS/cm) were not statistically significant. The breakdown voltage decreased about 28 percent with the increasing liquid conductivity from 0.01 mS/cm to 36 mS/cm according to both the simulation and experiment. This is because according to the circuit model, at the time point of electrical breakdown, the increasing rate of discharge voltage is zero

$$\left.\frac{dV_g(t)}{dt}\right|_{t=t_b} = 0 \tag{24}$$

Using equation (24) with equation (16) gives equation (25).

$$\mathrm{V_g}(t_b) = \frac{V(t_b)}{L\frac{d}{dt}\left(\frac{1}{R_p(t_b)}\right)+\frac{2R_S}{R_p(t_b)}+\frac{2R_S}{R_w}+\frac{2R_S}{R_3}+1} \tag{25}$$

Where t_b is the time point of the electrical breakdown. In equation (28), R_w decreased and the term $\frac{R_S}{R_w}$ increased with the increasing liquid conductivity. As a result, the breakdown voltage

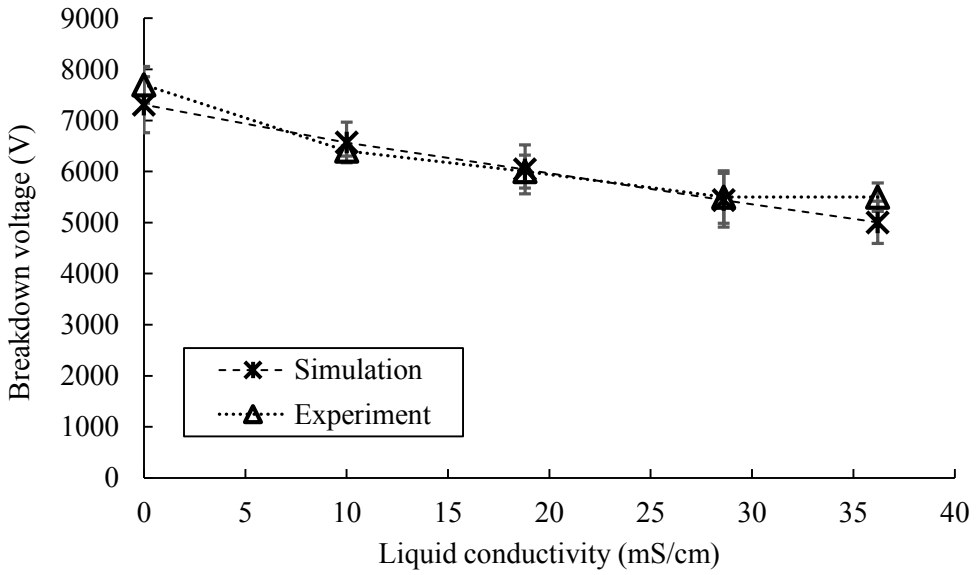

Fig 20. Comparison of breakdown voltage predicted by circuit model and the breakdown voltage measured from experiment. The voltage setting, the pulse width, and the frequency of power supplier were fixed at 20 kV, 50 ns, and 2 kHz, respectively. The liquid flow rate was fixed at 1mL/min. Argon was used as the carrier gas.

decreased since we assumed the applied voltage and conductivity of the plasma didn't change with liquid conductivity.

The decrease of breakdown voltage with the liquid conductivity can also be explained by the decrease of the dielectric relaxation time [49, 50]. The dielectric relaxation time is the time scale for the relaxation of charges, and the relaxation time of charge in liquid is approximately given by equation (26).

$$\tau_r = \frac{\varepsilon_r \varepsilon_o}{\kappa_w} \tag{26}$$

where ε_r is the relative dielectric constant of water, ε_o is the vacuum dielectric constant, and κ_w is the liquid conductivity. No charges were relaxed in the gas phase since the gas was not conductive before the breakdown. By increasing κ_w from 1 mS/cm to 36 mS/cm, the dielectric relaxation time decreased from about 70 ns to 20 ns. This suggested that the rate of mobile charge relaxation increased, and the rate of charge accumulation decreased with the increasing liquid conductivity [17]. As a result, the breakdown voltage dropped with the liquid conductivity.

Although the circuit model predicted the breakdown voltage accurately, the oscillations of the voltage and current waveforms were not simulated accurately. This is probably because the variation of electron density with time is different from the variation assumed in the model. It is possible that oscillations in the electron density lead to a secondary arc. Since the assumed electron density variation in the model did not include this possibility, the model does not exhibit oscillation.

The influence of pulse rise time on the electrical breakdown at high liquid conductivity was also investigated using the circuit model, and the results are shown in Figure 21. The same variation

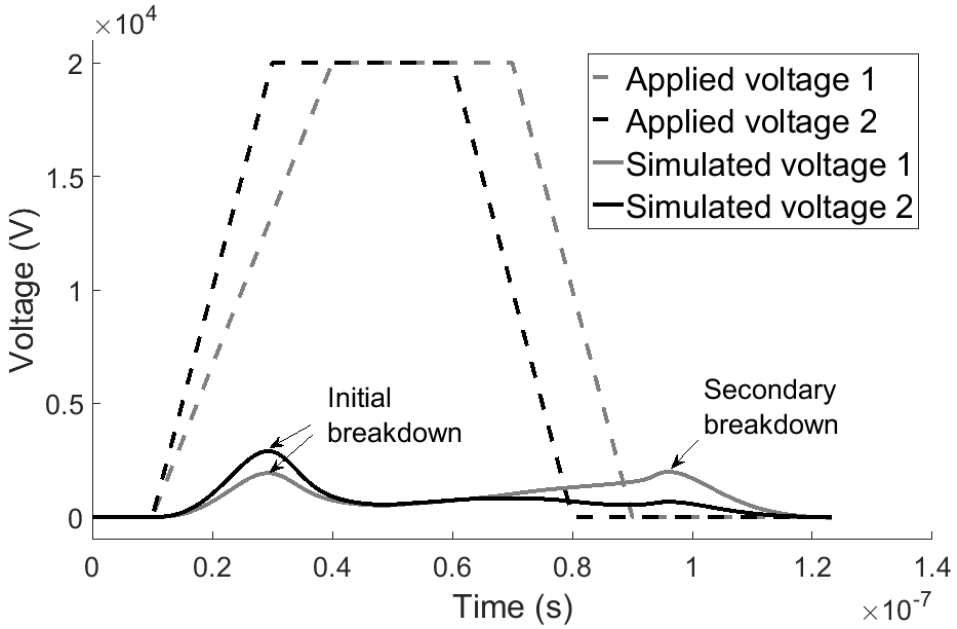

Fig 21. Simulated discharge voltage when two applied voltages with different rate of rise were used. The liquid conductivity was set to 36 mS/cm, and the electron density was assumed doesn't change under these two conditions.

of electron density with time was used in two cases with different applied voltage. For the plasma discharge generated in 36 mS/cm KCl solution, the breakdown voltage decreased with the increasing rise time of the applied voltage. According to equation (25), the breakdown voltage is positively related with the applied voltage at the time point of electrical breakdown. This implies that the applied voltage with shorter rise time can reach a higher value at the time point of breakdown than the applied voltage with longer rise time. Therefore, a shorter rise time results in a higher breakdown voltage across the electrode gap. On the other hand, the breakdown voltage will approach zero if the rise time of the applied voltage is continuously increased. The secondary pulse, shown in Figure 21, generated when the applied voltage 1 was used is due to the longer pulse width and the rapid decay of the electron density. In the case of applied voltage 1, the applied voltage remained high even after 80 ns, but the plasma channel was not conductive since we assumed the electron density rapidly decayed to zero after the initial breakdown, and as a result, the voltage built up again to generate the secondary breakdown.

The influence of the pulse rise time on the breakdown voltage can also be explained by considering the dielectric relaxation time. The dielectric relaxation time in water is about 20 ns when the liquid conductivity is 36 mS/cm, therefore the rate of charge accumulation at the electrode needs to be faster than the rate of charge relaxation in order to collect sufficient charge to generate a strong electric field. The rise time of the applied voltage directly reflects the rate of charge accumulation at the electrodes since the sharp increase in voltage is a result of charge accumulation. If the rise time of the applied voltage is longer than the dielectric relaxation time, the current or charge starts to flow through liquid before the voltage builds up and, as a result, the breakdown voltage drops. The longer rise time of the applied voltage causing a decrease of the breakdown voltage is one of the major reasons why the liquid conductivity tolerance of a microsecond pulsed power supply,

whose pulse rise time is usually several microseconds, is worse than the nanosecond pulsed power supply utilized here. By combining a nanosecond pulsed power supply and a water film plasma reactor, the system can tolerate water liquid conductivity at least as high as 36 mS/cm.

Conclusions

The influence of liquid conductivity on both argon and helium plasma discharges formed along a liquid water film was investigated. The liquid conductivity was adjusted by adding KCl to DI water, and the plasma properties, H_2O_2 production rate and energy yield, and the energy dissipated in the water were measured at five liquid conductivities.

The results showed that the plasma properties, including electron density, gas temperature, and plasma volume of the helium plasma didn't change significantly with liquid conductivity. Therefore, the production rate of H_2O_2 remained almost the same at the different liquid conductivities. However, since the increase of liquid conductivity reduced the resistance of the liquid film and caused the current to flow through the liquid, the energy dissipation in the liquid increased with the liquid conductivity. As a result, the overall energy yield (based upon total input energy) of H_2O_2 decreased about 16 percent with the liquid conductivity in the helium plasma, but the energy yield calculated using the discharge energy consumed by the plasma didn't change. For the argon plasma, the increased liquid conductivity changed the plasma properties. The electron density was about double at the highest conductivity of 36 mS/cm compared with DI water, but the increase of electron density from 0.01 mS/cm to 28 mS/cm was not significant. The plasma volume, determined using the discharge current and the measured electron density, showed a rapid decrease at 36 mS/cm, but the gas temperature did not change significantly with the liquid conductivity. The change in the argon plasma properties led to a decrease in $<\cdot OH>$ concentration predicted by a reaction model and the measured H_2O_2 production rate. As a result, the increase of energy dissipation into the liquid water and the decrease of discharge energy consumed by the plasma as the liquid conductivity was increased led to a decrease in overall H_2O_2 energy yield in the argon discharge, but the energy yield calculated based upon the discharge energy of the plasma, as in the helium case, remained the same under the different liquid conductivities.

The influence of liquid conductivity on the electrical breakdown was investigated using a circuit model. Both the simulations and experiments showed decreasing breakdown voltage with increasing liquid conductivity. This can also be explained by the decrease of dielectric relaxation time. The rate of charge relaxation increased with the increasing liquid conductivity, and the loss of charges through liquid undermined the electric field at the electrodes and resulted in a decrease in breakdown voltage. The simulation results also showed that the breakdown voltage is negatively related to the pulse rise time when the liquid was conductive. This is because the increase of the applied voltage needs to be faster than the relaxation of charges to reach the breakdown. The applied voltage generated by a nanosecond pulsed power supply has a shorter rise time than the microsecond pulsed power supply used in our previous work, therefore the nanosecond pulsed power supply has a much better liquid conductivity tolerance than the microsecond pulsed power supply. By combining the nanosecond pulsed power supply with the water film plasma reactor, a strong discharge can be generated when liquid conductivity is as high as 36 mS/cm where the energy yield of H_2O_2 only decreased less than 20%. This suggests the current plasma reactor system has the potential for treating polluted sea water and other highly conductive water.

Appendix. Analysis of variance

The one-way ANOVA test [51] was conducted separately for data from the argon and helium discharges using R to test whether the influence of liquid conductivity is statistically significant on input energy, discharge energy, H_2O_2 production rate and energy yield, and plasma properties. The sample size was chosen to be 3 based on the statistical power analysis [52], and the normality of the samples was tested by Shapiro-Wilk Normality Test using R [53]. The null hypothesis is that the liquid conductivity doesn't significantly influence the variables listed in Table A1 and A2. The p-value of the test was calculated and listed in Table A1 and Table A2. The null hypothesis was rejected when the p-value of the test is less than 0.05, and the rejection of the null hypothesis suggests the influence of liquid conductivity is statistically significant. The variables which are significantly affected by liquid conductivity were highlighted in the table.

Table A1. P-values of one-way ANOVA test for argon plasma

	Pr (>F)
Total Input Energy per pulse	0.298
Dissipated Energy in Liquid	4.46E-08
$E_{dissipation}$ / E_{tot} Percentage	9.73E-08
Discharge Energy of Plasma	8.09E-03
H_2O_2 Production Rate	5.96E-03
H_2O_2 Energy Yield in discharge	0.34
Overall Energy Yield	2.13E-03
Gas Temperature	0.896
Electron Density	4.64E-04
Plasma Volume	1.36E-05
Breakdown Voltage	2.65E-05
·OH Concentration	8.77E-04

Table A2. P-values of one-way ANOVA test for helium plasma

	Pr (>F)
Total Input Energy per pulse	0.178
Dissipated Energy in Liquid	6.02E-08
$E_{dissipation}$ / E_{tot} Percentage	5.92E-09
Discharge Energy of Plasma	0.861
H_2O_2 Production Rate	0.109
H_2O_2 Energy Yield in discharge	0.223
Overall Energy Yield	3.46E-03
Gas Temperature	0.723
Electron Density	0.492
Plasma Volume	0.0512
Breakdown Voltage	5.35E-04
·OH Concentration	0.158

A two-way ANOVA test was also conducted using R to consider the influence of carrier gas as well as the influence of liquid conductivity. The null hypothesis is neither liquid conductivity nor carrier gas significantly change the variables listed in Table A3. The variables whose p-values are less than 0.05 were again highlighted in the table.

Table 3. P-values of two-way ANOVA test

	Pr (>F)	
	Carrier Gas	Liquid Conductivity
Total Input Energy per pulse	1.80E-04	0.0819
Dissipated Energy per pulse in Liquid	0.0676	3.81E-15
$E_{dissipation}$ / E_{tot} Percentage	4.91E-03	1.21E-14
Discharge Energy of Plasma	2.42E-05	0.0762
H_2O_2 Production Rate	4.11E-15	5.26E-03
H_2O_2 Energy Yield in discharge	7.86E-12	0.112
H_2O_2 Overall Energy Yield	5.36E-13	1.68E-05

The results suggest the carrier gas significantly affects the variables listed in Table A3 except for the dissipated energy into the liquid.

Acknowledgements

This work was supported by the National Science Foundation (CBET 1702166) and Florida State University. JV was supported by Czech Science Foundation under contract 16-09721Y. BL was supported by the Czech Fulbright Commission and Florida State University.

Reference

[1] R. P. Joshi and S. M. Thagard, "Streamer-Like Electrical Discharges in Water: Part II. Environmental Applications," (in English), *Plasma Chemistry And Plasma Processing,* vol. 33, no. 1, pp. 17-49, Feb 2013.

[2] B. R. Locke, M. Sato, P. Sunka, M. R. Hoffmann, and J. S. Chang, "Electrohydraulic discharge and nonthermal plasma for water treatment," (in English), *Industrial & Engineering Chemistry Research,* vol. 45, no. 3, pp. 882-905, Feb 1 2006.

[3] P. J. Bruggeman and B. R. Locke, "Assessment of Potential Applications of Plasma with Liquid Water," (in English), *Low Temperature Plasma Technology: Methods And Applications,* pp. 367-399, 2014.

[4] B. Jiang *et al.*, "Review on electrical discharge plasma technology for wastewater remediation," (in English), *Chemical Engineering Journal,* vol. 236, pp. 348-368, Jan 15 2014.

[5] M. I. Stefan, *Advanced oxidation processes for water treatment: fundamentals and applications*. IWA Publishing, 2017.

[6] M. Magureanu, D. Piroi, N. B. Mandache, V. David, A. Medvedovici, and V. I. Parvulescu, "Degradation of pharmaceutical compound pentoxifylline in water by non-thermal plasma treatment," (in English), *Water Research,* vol. 44, no. 11, pp. 3445-3453, Jun 2010.

[7] H. H. Wang, R. J. Wandell, and B. R. Locke, "The influence of carrier gas on plasma properties and hydrogen peroxide production in a nanosecond pulsed plasma discharge generated in a water-film plasma reactor," (in English), *Journal Of Physics D-Applied Physics,* vol. 51, no. 9, Mar 7 2018.

[8] R. J. Wandell, " Development and characterization of a novel continuously flowing liquid film plasma reactor for chemical synthesis," Doctoral, Florida State University, 10196574, 2016.

[9] K. C. Hsieh, H. Wang, and B. R. Locke, "Analysis of Electrical Discharge Plasma in a Gas-Liquid Flow Reactor Using Optical Emission Spectroscopy and the Formation of Hydrogen Peroxide," *Plasma Processes and Polymers,* vol. 13, no. 9, pp. 908-917, 2016.

[10] P. J. Bruggeman *et al.*, "Plasma–liquid interactions: a review and roadmap," *Plasma Sources Science and Technology,* vol. 25, no. 5, p. 053002, 2016.

[11] K. Y. Shih and B. R. Locke, "Optical and Electrical Diagnostics of the Effects of Conductivity on Liquid Phase Electrical Discharge," (in English), *Ieee Transactions on Plasma Science,* vol. 39, no. 3, pp. 883-892, Mar 2011.

[12] P. Lukes, M. Clupek, V. Babicky, and P. Sunka, "Ultraviolet radiation from the pulsed corona discharge in water," (in English), *Plasma Sources Science & Technology,* vol. 17, no. 2, May 2008.

[13] T. Maehara *et al.*, "Influence of conductivity on the generation of a radio frequency plasma surrounded by bubbles in water," (in English), *Plasma Sources Science & Technology,* vol. 20, no. 3, Jun 2011.

[14] I. Kornev, F. Saprykin, and S. Preis, "Stability and energy efficiency of pulsed corona discharge in treatment of dispersed high-conductivity aqueous solutions," (in English), *Journal Of Electrostatics,* vol. 89, pp. 42-50, Oct 2017.

[15] A. Hamdan, K. Cernevics, and M. S. Cha, "The effect of electrical conductivity on nanosecond discharges in distilled water and in methanol with argon bubbles," (in English), *Journal Of Physics D-Applied Physics,* vol. 50, no. 18, May 10 2017.

[16] N. S. Midi, R. I. Ohyama, and S. Yamaguchi, "Underwater current distribution induced by spark discharge on a water surface," (in English), *Journal Of Electrostatics,* vol. 71, no. 4, pp. 823-828, Aug 2013.

[17] Y. Akishev *et al.*, "The interaction of positive streamers with bubbles floating on a liquid surface," (in English), *Plasma Sources Science & Technology,* vol. 24, no. 6, Dec 2015.

[18] T. T. Yan, X. X. Zhong, A. E. Rider, and K. Ostrikov, "Electric Breakdown in Liquids: Faster Ignition Using Less Energy," (in English), *Plasma Processes And Polymers,* vol. 10, no. 5, pp. 422-429, May 2013.

[19] K. Hsieh, H. J. Wang, and B. R. Locke, "Analysis of a gas-liquid film plasma reactor for organic compound oxidation," (in English), *Journal Of Hazardous Materials,* vol. 317, pp. 188-197, Nov 5 2016.

[20] R. J. Wandell and B. R. Locke, "Hydrogen Peroxide Generation in Low Power Pulsed Water Spray Plasma Reactors," *Industrial & Engineering Chemistry Research,* vol. 53, no. 2, pp. 609-618, 2014/01/15 2014.

[21] Y. T. Zhang and Y. H. Wang, "Modeling study on the effects of pulse rise rate in atmospheric pulsed discharges," (in English), *Physics Of Plasmas,* vol. 25, no. 2, Feb 2018.

[22] A. Komuro, R. Ono, and T. Oda, "Effects of pulse voltage rise rate on velocity, diameter and radical production of an atmospheric-pressure streamer discharge," (in English), *Plasma Sources Science & Technology,* vol. 22, no. 4, Aug 2013.

[23] T. Huiskamp *et al.*, "Spatiotemporally resolved imaging of streamer discharges in air generated in a wire-cylinder reactor with (sub)nanosecond voltage pulses," (in English), *Plasma Sources Science & Technology,* vol. 26, no. 7, Jul 1 2017.

[24] R. J. Wandell and B. R. Locke, "Low-Power Pulsed Plasma Discharge in a Water Film Reactor," (in English), *Ieee Transactions on Plasma Science,* vol. 42, no. 10, pp. 2634-2635, Oct 2014.

[25] H. W. R. Wandell, K. Tachibana, B. Makled, and B. Locke, "Nanosecond Pulsed Plasma Discharge over a Flowing Water Film: Characterization of Electrical and Plasma Properties and their Effect on Hydrogen Peroxide Generation," *Plasma Processes and Polymers,* vol. vol. inpress, 2018.

[26] R. J. Wandell, H. Wang, K. Tachibana, B. Makled, and B. R. Locke, "Nanosecond pulsed plasma discharge over a flowing water film: Characterization of hydrodynamics, electrical, and plasma properties and their effect on hydrogen peroxide generation," *Plasma Processes and Polymers,* vol. 15, no. 6, p. 1800008, 2018/06/01 2018.

[27] G. M. Eisenberg, "Colorimetric determination of hydrogen peroxide," (in English), *Industrial And Engineering Chemistry-Analytical Edition,* vol. 15, pp. 327-328, 1943.

[28] J. W. a. B. R. L. Huihui Wang and Robert, "The influence of carrier gas on plasma properties and hydrogen peroxide production in a nanosecond pulsed plasma discharge generated in a water-film plasma reactor," *Journal of Physics D: Applied Physics,* vol. 51, no. 9, p. 094002, 2018.

[29] P. Bruggeman, J. J. Liu, J. Degroote, M. G. Kong, J. Vierendeels, and C. Leys, "Dc excited glow discharges in atmospheric pressure air in pin-to-water electrode systems," (in English), *Journal Of Physics D-Applied Physics,* vol. 41, no. 21, Nov 7 2008.

[30] B. Peter *et al.*, "Optical emission spectroscopy as a diagnostic for plasmas in liquids: opportunities and pitfalls," *Journal of Physics D: Applied Physics,* vol. 43, no. 12, p. 124005, 2010.

[31] J. Vorac, P. Synek, V. Prochazka, and T. Hoder, "State-by-state emission spectra fitting for non-equilibrium plasmas: OH spectra of surface barrier discharge at argon/water interface," (in English), *Journal Of Physics D-Applied Physics,* vol. 50, no. 29, Jul 26 2017.

[32] J. Vorac, P. Synek, L. Potocnakova, J. Hnilica, and V. Kudrle, "Batch processing of overlapping molecular spectra as a tool for spatio-temporal diagnostics of power modulated microwave plasma jet," (in English), *Plasma Sources Science & Technology,* vol. 26, no. 2, Feb 2017.

[33] J. Luque and D. Crosley, "LIFBASE: Database and simulation program (v 1.6)," *SRI International Report MP,* pp. 99-009, 1999.

[34] S. Park, W. Choe, S. Youn Moon, and J. Park, "Electron density and temperature measurement by continuum radiation emitted from weakly ionized atmospheric pressure plasmas," *Applied Physics Letters,* vol. 104, no. 8, p. 084103, 2014.

[35] A. Y. Nikiforov, C. Leys, M. A. Gonzalez, and J. L. Walsh, "Electron density measurement in atmospheric pressure plasma jets: Stark broadening of hydrogenated and non-hydrogenated lines," (in English), *Plasma Sources Science & Technology,* vol. 24, no. 3, May 2015.

[36] S. Hofmann, A. F. H. van Gessel, T. Verreycken, and P. Bruggeman, "Power dissipation, gas temperatures and electron densities of cold atmospheric pressure helium and argon RF plasma jets," (in English), *Plasma Sources Science & Technology,* vol. 20, no. 6, Dec 2011.

[37] Y. J. Du, G. Nayak, G. Oinuma, Z. M. Peng, and P. J. Bruggeman, "Effect of water vapor on plasma morphology, OH and H2O2 production in He and Ar atmospheric pressure dielectric barrier discharges," (in English), *Journal Of Physics D-Applied Physics,* vol. 50, no. 14, Apr 12 2017.

[38] U. Kogelschatz, "Filamentary, patterned, and diffuse barrier discharges," (in English), *Ieee Transactions on Plasma Science,* vol. 30, no. 4, pp. 1400-1408, Aug 2002.

[39] G. J. M. Hagelaar and L. C. Pitchford, "Solving the Boltzmann equation to obtain electron transport coefficients and rate coefficients for fluid models," (in English), *Plasma Sources Science & Technology,* vol. 14, no. 4, pp. 722-733, Nov 2005.

[40] Y. T. Zhang, D. Z. Wang, and M. G. Kong, "Complex dynamic behaviors of nonequilibrium atmospheric dielectric-barrier discharges," (in English), *Journal Of Applied Physics,* vol. 100, no. 6, Sep 15 2006.

[41] A. A. Kulikovsky, "The Structure Of Streamers In N-2 .1. Fast Method Of Space-Charge Dominated Plasma Simulation," (in English), *Journal Of Physics D-Applied Physics,* vol. 27, no. 12, pp. 2556-2563, Dec 14 1994.

[42] Y. P. Raizer, "Gas discharge physics," 1991.

[43] J. Lou and Y. T. T. Zhang, "Analytical and Numerical Study on the Characteristics at the alpha-gamma Transition Point in Radio-Frequency Helium Discharges at Atmospheric Pressure," (in English), *Ieee Transactions on Plasma Science,* vol. 41, no. 2, pp. 274-279, Feb 2013.

[44] M. S. Simeni, A. Roettgen, V. Petrishchev, K. Frederickson, and I. V. Adamovich, "Electron density and electron temperature measurements in nanosecond pulse discharges over liquid water surface," (in English), *Plasma Sources Science & Technology,* vol. 25, no. 6, Dec 2016.

[45] P. Sunka *et al.*, "Generation of chemically active species by electrical discharges in water," (in English), *Plasma Sources Science & Technology,* vol. 8, no. 2, pp. 258-265, May 1999.

[46] B. Peter, S. Daan, G. Manuel Á, R. Robby, G. K. Michael, and L. Christophe, "Characterization of a direct dc-excited discharge in water by optical emission spectroscopy," *Plasma Sources Science and Technology,* vol. 18, no. 2, p. 025017, 2009.

[47] D. Seshie, "Effect of Conductivity Solution Salt Type on the Formation of Hydrogen Peroxide in Low Power Gas-Liquid Plasma," Master, Department of Chemical and Biomedical Engineering, Florida State University, Tallahassee, FL, USA, 2014.

[48] K. C. Hsieh, R. J. Wandell, S. Bresch, and B. R. Locke, "Analysis of hydroxyl radical formation in a gas-liquid electrical discharge plasma reactor utilizing liquid and gaseous radical scavengers," (in English), *Plasma Processes And Polymers,* vol. 14, no. 8, Aug 2017.

[49] Y. Yang, H. Zhang, C. Gong, G. Huang, and Y. Tu, "Effect of pulse width on streamer propagation of underwater corona discharge," *Plasma Processes and Polymers,* p. e1800028.

[50] B. R. Locke and S. M. Thagard, "Analysis and Review of Chemical Reactions and Transport Processes in Pulsed Electrical Discharge Plasma Formed Directly in Liquid Water," (in English), *Plasma Chemistry And Plasma Processing,* vol. 32, no. 5, pp. 875-917, Oct 2012.

[51] J. S. H. George E. P. Box, William G. Hunter, "Statistics for Experimenters: Design, Innovation, and Discovery, 2nd Edition," 2005.

[52] K. R. Murphy, B. Myors, and A. Wolach, *Statistical power analysis: A simple and general model for traditional and modern hypothesis tests*. Routledge, 2014.

[53] J. Royston, "Algorithm AS 181: the W test for normality," *Journal of the Royal Statistical Society. Series C (Applied Statistics),* vol. 31, no. 2, pp. 176-180, 1982.